WILEY-VCH

DOI: 10.1002/((please add manuscript number))
Article type: Review

Interface Engineering of Air Electrocatalysts for Rechargeable Zinc-Air Batteries

*Minghe Luo, Wenping Sun, Ben Bin Xu, Hongge Pan, Yinzhu Jiang**

M.H. Luo, Prof. W.P. Sun, Prof. H.G. Pan, Prof. Y.Z. Jiang
School of Materials Science and Engineering, State Key Laboratory of Clean Energy Utilization, Zhejiang University, Hangzhou, Zhejiang 310027, P. R. China
E-mail: yzjiang@zju.edu.cn

Prof. B. B. Xu,
Smart Materials and Surfaces Lab, Mechanical and Construction Engineering, Faculty of Engineering and Environment, Northumbria University, Newcastle upon Tyne, NE1 8ST, UK

Keywords: zinc air batteries, oxygen evolution reaction, oxygen reduction reaction, heterostructured electrocatalysts, single atom catalysts

In the face of high cost and insufficient energy density of current lithium ion batteries, aqueous rechargeable Zn-air batteries with the advantages of low cost, environmental benignity, safety and high energy density are spotlighted in recent years. The practical application of Zn-air batteries, however, is severely restricted by the high overpotential, which is associated with the inherent sluggish kinetics of oxygen evolution reaction (OER) and oxygen reduction reaction (ORR) of air electrocatalysts. Recently, engineering heterostructured/hybrid electrocatalysts by modulating the interface chemistry has been demonstrated as an effective strategy to improve the catalytic performance. Basically, there occur significant electronic effect, geometric effect, coordination effect, synergistic effect, and confinement effect at the heterostructure interface, which intensely affect electrocatalysts' performance in terms of intrinsic activity, active site density and durability. In this review, the recent progress on development of heterostructured air electrocatalysts by interface engineering is summarized. Particularly, the potential relationship between interface chemistry and oxygen electrocatalysis kinetics is bridged and outlined. This review would provide a comprehensive and in-depth understanding of the crucial role of the well-defined interfaces towards fast oxygen electrocatalysis, and would offer a solid scientific basis for the rational design of efficient heterostructured air electrocatalysts and beyond.

1. Introduction

Renewable energy technology has been reshaping the energy consumption landscape of modern society, which would alleviate the relay on traditional fossil fuels and mitigate the risk of deteriorating environment for a resilient future. [1] [2] To be a key issue, the efficient utilization of generated renewable electricity has put forward the demand for suitable energy storage technologies. [3] In this context, rechargeable batteries such as lithium-ion batteries (LIBs), have been brought into the spotlight. [4] [5] [6][7] However, the limited lithium deposit in nature cannot guarantee a feasible customized application in large-scale energy storage solutions at a cost-effective manner, [8] [9] not mention that some technical drawbacks such as constraint in undesired energy density and various safety concerns significantly still slow the commercialization of LIBs.[10] [11] Therefore, it is highly desirable to explore an alternative secondary battery technology to live up to the growing expectations. [12] [13]

Among the proposed alternatives, Zn-air battery (ZAB) with appealing energy density, low cost and high safety has aroused great interests. [14] [15] [16] The discharge and charge process are closely determined by the oxygen reduction reaction (ORR) and oxygen evolution reaction (OER), respectively. [12] [17]

During the discharge process:

ORR: O_2 (g) + $2H_2O$ (l) + $4e^-$ → $4OH^-$ (aq) (1)

During the charge process:

OER: $4OH^-$ (aq) → O_2 (g) + $2H_2O$ (l) + $4e^-$ (2)

Typically, the ORR and OER reactions involve multiple intermediates based on the complicated multi-step electron transfer mechanism and suffer from inherent sluggish kinetics. [18] [19] For ZAB with a theoretical voltage of 1.65 V, the working voltage is typically less than 1.2 V, and the charging voltage of over 2 V is required. Hence, the energy efficiency for current ZABs is remarkably low, typically less than 60%. [12] Therefore, exploring highly active air electrocatalysts is essential for realizing high performance ZABs. [20] [21]

To date, designing hybrid electrocatalysts with abundant rationally engineered interfaces has been regarded as an effective strategy to facilitate the reaction rate. [22] [23] Interface engineering as a strategy for composite formation can combine the merits of different materials, which is beneficial for exploring bifunctional active catalysts. [17] In addition, ORR and OER reactions are fundamentally different, involving different movement of electrons. The interplay at the interface can achieve simultaneous exposure of electron-rich and electron-deficient regions within a catalyst, which can facilitate both reduction and oxidation reactions. Benefiting from the significant interfacial interaction, which is unattainable for conventional catalysts, some transition-metal-based heterostructured catalysts even show high activity and stability that is comparable to noble-metal based composites [24] [25] [26] Although the critical role of interface haven been well demonstrated, a comprehensive discussion of interfacial effect is still rare. Previous reviews are mainly focusing on introducing the type or fabrication strategies. [18] [19] [27] Furthermore, the interfacial discussion center on single atom catalysts (SACs) is rarely mentioned. In this review, we first point out the importance of interface engineering for ZABs. Subsequently, technical aspects on how interfacial effects affect the oxygen electrocatalysis kinetics of catalyst and hence regulate the adsorption capability is discussed to clarify the fundamental mechanism of interface engineering. Then, we extend the discussion to SACs, where interfacial effect on stabilizing dispersed single metal atoms are introduced. Finally, future perspectives and existing challenges of interface engineering towards ZABs will be provide.

2. Interface Engineering of Air Electrocatalysts

Basically, there are two routes to improve the activity of electrocatalysts: (i) improving the intrinsic activity of each active site and (ii) increasing the number of active sites. [28] [29] From the former perspective, the bonding strength between the active site and the adsorbed molecules is referred as the descriptor to qualitative evaluate the catalyst activity, and the catalytic activity varies with the bonding strength as a volcano curve, according to the well-known Sabatier

principle. [30] An optimal catalyst should possess an intermediate bonding strength, neither too weak to activate the reactant, nor too strong to desorb the products. In principle, the typical strategy to modify the adsorption behavior of the intermediates is to adjust the electronic structure of the electrocatalysts. Thus, it is not difficult to understand why interface engineering has been regarded as an effective strategy to improve the catalyst activity of heterostructured electrocatalysts, since the electronic interaction at the interface plays a critical role in modulating the electronic structure of the active species. [24] [31] [32] When two components are in direct contact, the differences in Fermi levels, geometric structure and electronic affinity are able to trigger unexpected interfacial effects at the interfaces (**Figure 1**). The mismatch in Fermi levels can lead to charge redistribution at the interface and the created built-in electric field is essential for charge separation. [24] [33] As for the geometric structure, the dislocation of lattice constants can arouse compressive or tensile stain, which can shift the position of d-band center [34] and trigger the formation of defects. [35] Besides, the difference in electronic affinity can initiate the charge transfer through the interfacial chemical bonding. [36] Those effects improve the intrinsic activity of the catalyst by way of regulating the electronic structure. Another factor that restricts the catalyst activity is the scaling relation. [37] Based on the multi-step electron transfer mechanism, multiple reaction intermediates are involved in oxygen electrocatalysis. The adsorptions of these intermediates are correlated, and it is a formidable task to optimize the bonding strength simultaneously. [38] Interface engineering by combining catalysts with complementary activity together provides the opportunity to break such scaling law. It is noteworthy that, the above-mentioned effects do not operate separately, and as a rule, are directly or indirectly inter-related and together constitute the fundamentals of interface engineering. [39] [40]

With regard to increasing the number of active sites, downsizing the particle to achieve high exposed surface area is a realistic approach. [41] Particularly, single-atom catalysts (SACs), which symbolize downsizing the nanoparticles into monodispersed single atoms have been

extensively developed. [42] [43] However, the increasingly high surface energy generates severe self-aggregation when the particle size is reduced to atomic level. To ease/resolve this self-aggregation, introducing support material is critical and the metal-support interaction across the interface plays a key role in stabilizing SACs. [43] [44] [45] [29] To strengthen the interaction, introducing coordinating sites into substrates is the commonly used strategy, and carbon-supported catalysts containing N-coordinated transition metals (M-N-C) is the most extensively studied single-atom catalysts for Zn-air batteries. [46] [47] Engineering interface through localised confinement effect is capable of achieving the maximum density of exposed active sites and of preserving the structure integrity of the active sites.

As for the synthesis of heterostructured composite with well-defined interface, there are various synthetic routes such as electrodeposition, photochemical deposition, colloidal strategies and atomic layer deposition (ALD).[48] Basic seeded growth is the common principle in designing hetero-interface. In such case, pre-formed nanoparticle can serve as "seeds", functioning as substrates for the attachment and growth of secondary different material. It is remarkable that when secondary material is deposited on the pre-formed substrate, the doposition mode varies with the change of ΔG_s, total Gibbs free surface energy change function, which is associated with the surface energy of materials (γ_1 and γ_2) and their match degree ($\gamma_{1,2}$, solid-solid interfacial energy).[49]

$$\Delta Gs = \gamma_1 - \gamma_2 + \gamma_{1,2} \quad (3)$$

When $\Delta G_s > 0$, the deposition of secondary material is in compliance with the layer-by-layer mode, achieving a uniform coverage. In another case, the deposition is inclined to form discrete island.

Since interface plays such an important role in improving the performance, how to construct a robust interface that ensures heterostructured catalytic stability during long-term operation is the focus concern of researches. In this point, targeted select of substrates and the loaded substance to guarantee strong interaction between them is essential. [48] [50] [51] Lim *et al.* has

demonstrated that the stability of β-$Ni(OH)_2$/NiO composite depended on the stack mode of β-$Ni(OH)_2$ on surface NiO. When $\{111\}_{fcc}$-faceted NiO was selected as substrate, the binding strength between β-$Ni(OH)_2$ and NiO was stronger than that of $\{100\}_{fcc}$ and $\{110\}_{fcc}$-faceted NiO, leading to the suppressed exfoliation of β-$Ni(OH)_2$ sheets after 10 hours treatment in alkaline media. [52] In addition, long-term stability test is necessary for accurately estimating the durability of heterostructured catalyst. [53] Since if heterointerface is deteriorated during catalysis, it possible to reflect in current density change at an applied overpotential. [54]

To identify the relationship between interface and performance, the accurate characterization of physical/chemical properties of heteostructured composite has become an urgent but difficult task. As mentioned above, due to the difference in Fermi levels, the electronic interaction between the contacted phase is expected, which has a significant impact on electrocatalysis. In such cases, X-ray-based spectroscopic techniques are important tools to detect the charge density change upon interface formation. [48] Characterizations such as X-ray absorption fine structure (XAFS), X-ray photoelectron spectroscopy (XPS) and X-ray absorption spectroscopy (XAS) can be carried out to analyze the valence and local environment of metal species. Besides, Kelvin probe force microscopy (KPFM) can also be used to detect surface electronic properties, while other scanning probe-based characterizations such as scanning tunneling microscopy (STM) and atomic force microscopy (AFM) are considered for surface/interface physical properties identification. [55] [56] In addition, when graphene and two-dimensional materials are involved, Raman spectra plays important role in understanding of heterostructure. [56] It is noteworthy that no single characterization is able to identify the real physical/chemical state of composite. Hence, mutual corroboration among the different characterizations and theoretical simulation are remarkably important.

3. Effects for interface engineering

Interface is typically referred to the boundary between two different components. When dissimilar materials with different geometrical and energy band structure are contacted,

interface region has been demonstrated to exhibit fundamentally different physicochemical characteristics from that of its bulk counterparts. [33] This so called "interfacial effects" play a central role in improving the performance of OER, ORR, as well as the Zn-air battery. In this section, we make classified discussion on these interfacial effects according to the different mechanisms. The key focus is placed on how these effects affect oxygen electrocatalysis kinetics and hence improve the intrinsic activity.

3.1. Electronic Effect

3.1.1. Space Charge Effect

The intrinsic activity of catalyst is closely bound up with its electronic structure. After forming a nanointerface between two dissimilar materials, the mismatches in Fermi levels (E_f) or work functions will be likely to lead to charge transfer across the interface, which accompanies by the break of electrical neutrality and the variety of charge density. [39] Specifically, the electrons will flow from the component with high E_f to the one with low E_f until reaching equilibrium. The accompanied energy band bending at the interface controls the flow of charge carriers. [57] [58] Moreover, the accumulation or depletion of mobile charges will create a built-in electric field with two opposite charged regions. Such charged regions near the interfaces have the impact on the chemisorption rates of the reactants (O_2 for ORR, and OH^- for OER). [32] Qian *et al*. demonstrated that when n-type Fe-Ni-LDH was coupled with p-type CoP, positively charged centers could be created at the Fe-Ni-LDH surface as the result of the electron transfer from Fe-Ni-LDH to CoP (**Figure 2**a). By the aid of DFT calculations, it was concluded that the adsorption energy of OH^- on the surface of CoP coupled Fe-Ni-LDH was 1.31 eV lower than individual Fe-Ni-LDH. Hence, the OER performance of Fe-Ni-LDH/CoP was increased 10-fold. [32] As depicted in **figure 2b**, Fe-Ni-LDH/CoP showed a large turnover frequency of 0.131 s^{-1}, while only 0.0177 was achieved by Fe-Ni-LDH. An *et al*. synthesized $NiFe_2O_4/FeNi_2S_4$ heterostructured nanosheets, which has been by far the most efficient catalyst for ZABs with neutral aqueous electrolyte (**Figure 2**c). [24] The XPS peaks of O1, O2 and O3

of $NiFe_2O_4/FeNi_2S_4$ presented negative shifts compared with pristine $NiFe_2O_4$, while the binding energies of S $2p_{1/2}$ and S $2p_{3/2}$ showed positive shifts compared with $FeNi_2S_4$, which strongly indicated the charge transfer occurring on the interface. The electronic interaction between the contacted domains was further validated by DFT calculations, as shown in **Figure 2**d. The differential charge density data revealed that oxygen was more likely to adsorb on surface Ni around the interface. In addition, the oxygen adsorption energy was modified at the interface, which is crucial for facilitating the OER and ORR kinetics. As a result, for OER performance, the composite showed a small overpotential of 253 mV to achieve the current density of 10 mA cm^{-2}. As regards the ORR performance, $NiFe_2O_4/FeNi_2S_4$ showed an onset potential of 0.715 V and a half-wave potential ($E_{1/2}$) of 0.507 V, which was superior than $NiFe_2O_4$ and $FeNi_2S_4$ (onset potential of 0.648 V for $FeNi_2S_4$ and 0.503 V for $NiFe_2O_4$; $E_{1/2}$ of 0.361 V for $FeNi_2S_4$ and 0.273 V for $NiFe_2O_4$). Once applying such heterostructured $NiFe_2O_4/FeNi_2S_4$ as the air catalyst, the Zn-air battery with neutral aqueous electrolyte showed a peak power density of 44.4 mW cm^{-2} and an excellent cycling stability with no obvious decay over 900 cycles (**Figure 2**e). Similarly, Ma *et al*. has synthesized a heterostructured Fe/Co bimetal phthalocyanine. [50] Through DFT calculation, it was demonstrated that such interface engineering strategy has led to the elongated Fe-N length, increased electron density around Fe sites and reduced energy gap between the HOMO (highest-occupied molecular orbital) and LUMO (lowest-unoccupied molecular orbital). Consequently, the heterostructured bimetal phthalocyanine showed a superior performance with an onset potential of 0.971 V and a half-wave potential of 0.879 V.

3.1.2. Charge Separation

The solar energy, an inexhaustible energy source that widely used, has enabled a novel application in ZABs known as photo-enhanced Zn-air battery, which can be considered as the combining of photochemical and electrochemical (**Figure 3**a). [33] [59] When the photo-electrode is irradiated by light, electrons are excited to a high energy state from valence band (VB) to

conduction band (CB), generating electron-hole pairs. [60] Within Zn-air battery, O_2 can be trapped by photo-excited electrons and be reduced to O^{2-} radicals. While OH^- can be trapped by photo-induced holes, facilitating the formation of hydroxyl radical species (**Figure 3**c). [59] Therefore, the chemisorption rates of the reactants O_2/OH^- are altered, which determine the performance of the Zn-air battery. However, the photo-excited electron-hole pairs are easily to recombine. Therefore, efficient charge separation must be considered when designing a photo-assisted Zn-air battery.

Constructing a semiconductor heterojunction system is an effective way to realize efficient charge separation. The heterojunctions formed between two different semiconductors can be classified into three types based on the relative positions of CB and VB. [60] [61] Among them, type II heterojunction with a staggered gap is desirable (**Figure 3d**), where photo-electrons are apt to transfer from CB(A) to CB(B) driven by internal electric field, with holes accumulating at semiconductor A. In addition to the interface between two semiconductors, charge separation phenomena can also occur via Schottky contact at the metal-semiconductor interface (**Figure 3**e). [62] [63] The Schottky barrier offers a one-way flow route from semiconductor to the metal for electron transfer, thus promoting effective charge separation.

Utilizing above charge separation mechanism, Lv *et al.* have, for the first time, proposed a photo-responsive functional catalyst for Zn-air battery by coupling n-type N-doped carbon nanotubes (NCNT) with p-type $Ni_{12}P_5$ nanoparticles. [59] Due to the created p-n junctions, electron-hole pairs were generated and separated when $Ni_{12}P_5$ adsorbed lights. The photo-generated electrons which were transferring to NCNT could facilitate oxygen reduction and the remaining photo-generated holes could facilitate OH^- oxidation; therefore, the performance of Zn-air battery was improved by light irradiation. Consequently, upon irradiation, the overall oxygen electrode activity ΔE ($\Delta E = E_{OER,\ j=10} - E_{ORR,\ 1/2}$) was decreased from 0.82 to 0.80 V. When $Ni_{12}P_5$@NCNT catalyst was adopted as air electrode, the photo-assisted Zn-air battery showed a charge potential of 1.90 V and a discharge potential of 1.22 V (voltage drop of 0.68

V with round-trip efficiency of 64.2%) at a current density of 10 mA cm^{-2}. From the other side, Zn-air battery without the light irradiation showed a potential drop of 0.75 V with an efficiency of 61.3% **(Figure 3**b).

3.1.3. Electron Penetrating

For most cases, Zn-air batteries are operating in alkaline condition and to achieve the maximum electrolyte conductivity, a high concentration KOH solution (about 6-7 M) is used as a standard set. [14] However, comparing with precious metal catalysts, transition metal catalysts are more unstable under harsh conditions. To address the unstable issue for the non-precious metal catalysts, a concept of chainmail catalyst has emerged recently (**Fig. 4**a), [64] where metals are encapsulated into the carbonous shell to avoid to be exposed in strong alkalinity directly. Through the metal-carbon interaction at the interface, electrons can flow from the encapsulated metals to the external carbonous shell to trigger outer surface activity (usually within the range of three to four carbon layers, **Fig. 4**c). [65] Deng *et al.* reported that the transferred electrons can modify the electronic states of C atoms, increasing the Fermi level and lowering the work function. [66] In addition, the local dipole accompanied by charge transfer can lead to the redistribution of partial charge. The overall charge transfer induced modifications are expected to lower kinetic energy barriers and increase the chemical reactivity of composite. Furthermore, a case study of Ru confined carbon nanotubes indicated that when Ru was confined on the inner of the CNT, 2.41 electrons was transferred from Ru to the CNT which was higher than that of Ru confined on the outside of the CNT (1.66 electrons, **Fig. 4**b). [67] This means the electronic state of composite can be maximum altered in the case of chainmail catalyst, comparing with non-encapsulated condition.

Benefiting from the chainmail protection effect, the alkali Zn-air battery with a superior stability can be realized. Using a two-stage encapsulation method, Xing *et al.* synthesized a type of chainmail catalyst in which NiFe core with the size of 7.8 nm was encased in graphitic layers (denoted as NiFe@NC_x). [68] The electron penetrating from the metal core to the carbon

outer layers was confirmed by the evolution of C 1s, Fe 2p and Ni 2p signals. Specifically, a new peak located within the range of 282.2-282.7 was detected in the XPS spectrum of C 1s and a shift of the signals of Fe and Ni was observed. As for the catalytic activity for ORR, NiFe@NC_x composite showed an onset potential of 1.03V and a higher $E_{1/2}$ of 0.86 V. In addition, after cycling for 20000 cycles, only 5 mV shift was detected for half-wave potential. By employing NiFe@NC_x as air-electrode, the Zn-air battery showed a gravimetric energy density of 732.3 Wh kg_{Zn}^{-1} while only 543.2 Wh kg_{Zn}^{-1} was delivered for Pt/C+IrO_2-based battery. At a current denisty of 50 mA cm^{-2}, the charge-discharge overpotential was 0.78 V, which was higher than that of Pt/C+IrO_2-based battery (1.1 V at 50 mA cm^{-2}). For the cycling performance of NiFe@NC_x, only 0.29 V increase was detected after cycling for 205 cycles.

3.2. Geometric Effect

3.2.1. Strain

Strain effect is one of the structural factors that dominates the electrocatalyst performance. When two dissimilar materials with different lattice constants are in direct contact, lattice strain can be generated near the interface region due to the lattice mismatch between the adjacent phases **(Figure 5**a). [69] [40] [39] Such strain can be defined in several forms, which corresponds to a particular circumstance. [70] In the case of small strains, for example, the definition of the strain along a line is $(l_f - l_i)/l_i$, where l_f and l_i refers to the atomic bond length in the final state and the initial state, respectively. However, the accurate evaluation of atomic bond length remains a challenge. In consideration that the variation of the bond length is closely related with the lattice parameter; therefore, degree of the lattice strain (s) can be determined by the following equation with core-shell structured composite as the model: [34]

$$s = \left(\frac{a_{shell} - a_{bulk}}{a_{bulk}}\right) * 100 \qquad (4)$$

Hereby, a_{shell} and a_{bulk} are the corresponding different lattice parameters of core/shell, which can be determined by XRD technology. This equation gives the possibility to quantify the surface lattice strains and correlate the structure and the activity of catalyst.

The generated lattice strain, either compressive or tensile, is expected to regulate the surface electronic structure by altering the interatomic distance. [34] [71] For instance, for ORR reaction, the induced tensile lattice strain can bring about a up shift of the d-band center, which usually leads to the enhancement of interaction between the active sites and the adsorbates **(Figure 5**d). [72] Thus, the step of O-O bond breaking may facilitate. Opposite to the tensile lattice, the compressive strain will cause the down shift of the d-band center and the weakened interaction may benefit the selectivity for H_2O_2. [73] This general trend has been proven experimentally in many practices and have been served as guidance for the catalyst designing from the perspective of surface strain control. However, it is noteworthy that the above-mentioned general trend is inapplicable to the early transition metals with a less than half-filled d band. According to the report from Schnur *et al.*, the lattice expansion of early transition metals was accompanied by the down shift of the d-band center, as well as a lower adsorption energy, which was opposite to the late transition metals. [72]

By constructing a core/shell structure to induce strain, Bu *et al*. obtained PtPb/Pt core/shell nanoplates with large biaxial strains on the exposed Pt(100) facets. [74] The DFT calculation predicted that the induced biaxial strain could alter the strength of the Pt-O bond to an optimized value **(Figure 5**b). Hence, the ORR activities of PtPb/Pt nanoplate was 33.9 times greater than commercial Pt/C catalyst and the PtPb/Pt nanoplate showed an excellent stability even after 50000 sweeping cycles **(Figure 5**c). Similarly, Xiao *et al.* obtained core-shell structured Pd_2FeCo@Pt/C with the lattice contraction of 2.24%. [75] On account of the lattice contraction induced adsorption strength decrease of the Pd surface, when Pd_2FeCo@Pt/C was applied as air electrode for Zn-air battery, the battery delivered a peak power density of 308 mW cm^{-2} and a superior cycling stability with only 38 mV potential loss after 100h.

3.2.2 Defect

It has been proven both empirically and theoretically that surface with defects may be more active in catalytic property than non-flawed surface. [76] By interface engineering, defects can form accordingly to relieve the strain energy and stabilize interfacial structure. [77] Oxygen vacancies are the most common type of defects due to its low formation energy in transition metal oxides. [76] When oxygen vacancy is introduced, the electrons that previously occupied O 2p orbital become delocalized, suggesting the high activity of surface with oxygen vacancy **(Figure 6**a). [78] The existence of oxygen vacancy can create some new electronic states in the bandgap, which is significant in improving electronic conductivity, as shown in **Figure 6**b. [79] Besides, defects and the related structure disorder can provide numerous unsaturated atoms as atomic-traps to enhance the adsorption of oxygen intermediates.

The crucial role of defects in adjusting the activity of catalyst has been fully verified in previously reported work. [77] [80] [81] For example, Jiang *et al.* has successfully synthesized the graphitic carbon framework supported "Janus" nanoparticles (Co/Co_3O_4@PGS). [81] The "Janus" feature of immobilized particle was vividly indicated in **Figure 6**d, which showed the distinct double sets of interplanar spacing domains within the same particle. The lattice fringe (0.177 nm) of e domain was indexed to the (200) plane of metallic Co while the lattice fringe (0.199 nm) of f domain was indexed to the (400) of Co_3O_4. The oxygen defects (highlighted by dashed circles) were detected near the nanointerface domain (highlighted by dashed line) and some morphological distortions were found in graphitic carbon framework. The formation of oxygen defects was further supported by XPS analysis. It showed that the atomic ratio of Co^{2+} and Co^{3+} in Co/Co_3O_4@PGS was 0.72 which is higher than that in Co_3O_4@PGS (0.5). The defect-rich interfaces functioned as atomic traps could be beneficial for the bonding of oxygen reactants and the constructed interface could functioned as highway for the transfer of electrons. Therefore, Co/Co_3O_4@PGS composite showed a satisfied performance with a $E_{1/2}$ of 0.89 V for ORR and a low potential of 1.58 V to achieve the current density of 10 mA cm^{-2}. In addition,

Zn-air battery with Co/Co_3O_4@PGS as air electrode showed a narrow voltage gap of 0.91 V at 10 mA cm^{-2}, a power density of 118.27 mW cm^{-2} and a superior stability (over 800 h at 10 mA cm^{-2}, **Figure 6**c).

3.3. Coordination Effect

Doping heteroatoms into carbon material (e.g., nitrogen-doped) is a practical strategy to regulate the electronic state of C atoms in doped area and thus adjust the performance. [19] Beyond that, the N-doped carbon material with the high affinity of nitrogen can also be combined with metal atoms. [82] [83] The specific coordination configuration participates in constructing the efficient active site especially for ORR reaction. For instance, tremendous works have demonstrated that macrocycle complexes with FeN_xC_y moieties are satisfied molecular catalysts for ORR, even though bulk Fe itself has no apparent activity. [84] Additionally, the formed interfacial chemical bonding can also alter the coordination state and valence state of metal atoms. When Pt are coordinated to the N atom with high electronegativity, the electron withdrawal from the Pt 5d orbitals lead to a high valence state, which further affect its adsorption of relevant species (O*, OH*, OO*, and OOH*) on surface active sites. [84] [85] It should be noted that the electron interaction between the metal and the N-doped carbon support depends on the types. Yang *et al*. have reported that for metal Co, graphitic-N as electron donor doping is difficult to form chemical bond with transition metal ion due to the electron repulsion. In addition, the chemical bond between pyrrolic-N and transition metal ion was weak with negligible electron transfer. It was pyridinic-N that play a dominant role in oxygen electrocatalysis and a certain number of charge transfer was detected from Co to N in pyridinic-N-Co bonding. [36]

The altered coordination number is another factor that influence the adsorption ability of catalysts. In the case of $NiCo_2O_4$, four-fold coordination was stable for Co. Therefore, adsorption of relevant species (O* or OH*) on surface Co sites to form four-fold coordinated Co was favorable (exothermic) while formation of OO* (ORR, overpotential 0.34 V) and

OOH* (OER, overpotential 0.50 V) were endothermic (**Fig. 7a)**. However, when interfacial Co atoms were coordinated with pyridinic N, the N-coordinated Co was stabilized in composite with four-fold coordination. Given the fact that Co tended to occupy the tetrahedral field in regards to octahedral field for Ni, OO* and OOH* would co-adsorb on the Co site and its adjacent Ni site in NiCo/Pyri-NG. As a result, formation of OO* (ORR)/OOH* (OER) converted to an exothermic process in this situation (**Fig. 7c)**. In this situation, the overpotential of ORR and OER process for NiCo/Pyri-NG were 0.22 and 0.29 V, respectively. Therefore, the Zn-air battery with NiCo/Pyri-NG as active catalyst showed a high open circuit voltage of 1.49 V and the discharge/charge potential was observed as low as 0.8 V. Besides, the charge/discharge curves showed that battery could offer a peak power density of 103 mW cm^{-2} at 140 mA cm^{-2} **(Fig. 7b)**. [36]

3.4. Synergistic Effect

Catalyst with single component that works to either ORR or OER is generally unsatisfied to the other reaction. [86] For example, Pt as the efficient ORR catalyst can be oxidized under OER condition, and OER catalyst, such as Ir or Ru-based catalyst, is insufficient to ORR. Therefore, it is natural to put forward the concept of exploring bifunctional active catalyst from incorporating multiple targeted components, since formation of polyelemental catalyst can combine the merits of different component. [17] Based on this so called "synergistic effect", Ma *et al.* have proposed a bifunctional Janus catalyst via selective combining the single atom Fe sites and Ni sites. [87] As shown in **figure 7**d, the outer Fe sites were responsible for ORR reaction while inner Ni sites were OER active. And comparing with benchmark Pt/C+RuO_2, which was just simply mixing, the effective interface engineering ensured the tight contact of Ni/Fe based configurations on hollow graphene. Hence, a satisfied Zn-air battery with high energy efficiency and cycling stability was achieved (200h at 10 mA cm^{-2}).

For 4-electrons ORR/OER reactions, the linear scaling relations between multiple intermediates pose a serious limitation to develop efficient ORR/OER catalysts. [37] [88] To

achieve an ideal catalyst, all the intermediate bonding strength should be optimal, neither too weak or too strong. However, the adsorption strength of these intermediates is correlated. Therefore, it turns out to be an impossible task to optimize the bonding strength simultaneously for a single component catalyst. Surprisingly, some previous work has demonstrated that such scaling law is possible to be broken by using synergistic effect arises from the heterointerface. [38] Sun *et al.* has selectively combined the IrO_2 particles and $Ni(OH)_2$ nanosheets to form the heterostructure composite. Unlike that the adsorption of OER intermediates limited to a single active site, the intermediates OH* and O* were more likely to adsorb on $Ni(OH)_2$/NiOOH and IrO_x, respectively. The two intermediates were combined at the heterointerface and the formation of OOH* was accelerated (**Fig. 7**e). Therefore, scaling relations was eventually brooked and bonding strength of intermediates were optimized simultaneously. The Ir/$Ni(OH)_2$ composite showed superior OER performance (overpotential of 224 mV to deliver 10 mA cm^{-2}) than both single $Ni(OH)_2$ (437 mV) and Ir particles (**Fig. 7**f).

The term "synergistic effect" is a broad, imprecise concept. Besides above-mentioned application scenarios, active metal oxide species coupled with inert but conductive carbonaceous substrates to improve catalysis performance can also attribute to the "synergistic effect". [89] It is worth reminding that, to clarify the origin of performance improvement more clearly, the usage of "synergistic effect" should be more rigorous with solid in-depth discussion.

4. Interface Engineering towards SACs

Recently, single-atom catalysts (SACs) with isolated metal atoms dispersed on the support and modulation of interface chemistry at atomic scale have attracted intensive research interests (**Fig. 8a**). [42] [44] [45] Similar to the "interfacial effect" stated above, electronic interaction at atomic interface is also expected to enhance the intrinsic activity of SACs. For example, Chen *et al.* synthesized a catalyst with single iron atomic sites dispersed in N, P, S co-doped carbon polyhedron (denoted as Fe-SAs/NPS-C). [90] On the basis of charge density differences and Bader charge analysis, it was found that, owing to the charge donation from the surrounding P,

S atoms, the Fe centers of Fe-SAs/NPS-C became less positive, and hence showed less intense interaction with OH^* and better ORR performance (**Fig. 8b**). Considering that this interface engineering-intrinsic activity relationship has been discussed above, the discussion of the interface engineering towards SACs is mainly focusing on how metal-support interaction enables the stabilization of single atoms.

It is well known that the migration and agglomeration of isolated metal atoms are critical issues that lie ahead of SACs. The interaction between the isolated atoms and the support is a key factor in achieving the synthesis of SACs and determining the durability of catalyst. [29] Introducing coordination sites to anchor metal precursors is effective to realize the atomically dispersed active sites. [90] [91] For carbon-supported catalyst with N-coordinated transition metal atoms (M-N-C), the key point is the strong interaction between metal species and N atoms with long pairs of electrons. [43] It is expected that the d-orbitals of transition atoms and the 2p-orbitals of N can hybridization. Therefore, isolated atoms can be two-fold or four-fold coordinated by neighboring N atoms to form the moieties, metal-N_2/N_4-C, which can be well detected by X-ray adsorption spectroscopy. Benefiting from the such strong interaction, M-N-C type catalysts are the most extended studied single-atom catalysts for Zn-air batteries, especially for transition metal Fe and Co. [92] [93] [94] Peng *et al*. synthesized a well-designed atomically dispersed Fe-N-C centers through a pyrolysis-free path (denoted as pfSAC-Fe). [95] The data from X-ray absorption near-edge structure (XANES) indicated the formation of N-coordinated Fe atoms. In the Fourier transform analyses, a main peak in the curve of pfSAC-Fe was attributed to the Fe-N scattering paths, while the peak of Fe-Fe located at 2.2 Å was not detected. In addition, by further simulating the extended X-ray absorption fine structure (EXAFS), signals of the two-body backscattering path of Fe-N was detected in pfSAC-Fe. This metal-support interfacial interaction ensures the high stability of SACs when it was applied for Zn-air battery. Accordingly, Zn-air battery based on pfSAC-Fe composite showed an excellent cycling life over 300 h at 5 mA cm^{-2}, and even at a high current density of 100 mA cm^{-2}, a life

over 300 min was maintained. Furthermore, as shown in **Fig. 8d**, only a small voltage decay was detected over 30 h when the current density was periodically changed from the 5 to 40 mA cm^{-2}.

Another strategy used for restricting the migration of metal atoms, is to construct defective support with a high density of defects. The introduced defects can provide numerous vacancies and/or unsaturated atom sites, which can serve as trapping sites to capture metal precursors (**Fig. 8e)**. [29] [96] Defect engineering can significantly improve the overall metal loading on graphene support, as the edge is the only adsorptive sites. For example, a high density of atomic Ni was achieved with a defective graphene as support (A-Ni@DG, about 6.3×10^5 Ni/μm^2), and for comparison, when pristine graphene was selected as THE support, the density of Ni was about 3.6×10^5 Ni/μm^2. [97] X-ray adsorption spectroscopy and HADDF-STEM images revealed that atomic Ni was trapped in the Di-vacancy defect via the coordination between the metal atom and the 2π antibonding state of the nearby carbon atoms (**Fig. 8f)**. Furthermore, LCF simulation and DFT calculation revealed that Ni anchored on defect area is rather thermodynamic stable. Based on such robust immobilization of Ni atoms on the defective support, the A-Ni@DG presented a high stability for long-term reactions and after 10 hr of continuous OER at a current density of 5 mA/cm^2, the voltage decay was negligible.

5. Outlook

In this review, a periscope summary of interfacial engineered air electrocatalysts for Zn-air battery is provided from two perspectives: improving the intrinsic activity and increasing the number of active sites. In the section of intrinsic activity, more attention is focused on how interfacial interaction influences the oxygen electrocatalysis kinetics of the catalysts. Specifically, the electronic effect, geometric effect and coordination effect are expected to have significant impact on the electronic structure of the active species, and hence improve the intrinsic activity accordingly. Meanwhile, the synergistic effect enabled by the multiple compositions at the interface is also of great significance to the enhanced catalytic activity by

breaking scaling relationship. In the section of increasing active sites number, the interfacial engineering enabled SACs synthesis is scoped to envisage how to use interfacial interaction to stabilize single atoms.

Despite above advancements in improving the performance of Zn-air battery through interface engineering, challenges remain in the following contexts:

(1) In-depth in-situ/ex-situ characterization of heterointerface and understanding of relevant mechanisms. In most cases, the characterizations of heterointerface focuses on the state before the electrocatalysis. However, it is essential to comprehend how heterointerface evolves during the reaction for better understanding the role of heterointerface. Therefore, post-reaction analyses and advanced in-situ characterization techniques are needed to reveal the evolution of geometry structure and electronic structure of electrocatalysts as well as the adsorption behaviors of reaction intermediates under working conditions. On this basis, we can gain more comprehensive understanding of the relevant reaction mechanisms and performance enhancement mechanisms.

(2) Theoretical study of interfacial effect. Integrating theoretical analysis with experimental support are beneficial to elaborate the effect of interface and hence give a guidance to novel heterostructured material design. However, for heterogeneous heterostructured catalysts, the active sites are non-uniform in nature [29]. Currently, there is still a gap between the theoretical model and practice electrocatalyst. To bridge this gap on the structure-performance relationship, a well-defined model system for theoretical calculation is needed.

(3) Constructing a stable triple-phase interface. Contrary to the electrocatalytic measurement in a three-electrode system with the relatively ideal electrolyte, especially O_2-saturated electrolyte for ORR, a stable three-phase interface (electrolyte-solid catalyst-gaseous oxygen) need to be constructed in the practical application of Zn-air battery due to the extremely low O_2 solubility. [51] This means additional challenges such as gas diffusion ability and wettability of air electrode need to be considered. In this regard, interface engineering to regulate the

hydrophobicity and construct mass transport channel also merit attention.

(4) Interface engineering for neutral aqueous Zn-air battery. Comparing with the alkaline condition, the application of interface engineering for neutral aqueous Zn-air battery is relatively rare. For OER in neutral condition, the water dissociation may participate in the reaction process since the reactant OH^- is insufficient. Through referring to the case of alkaline hydrogen evolution reaction, which integrating the hydroxyl adsorption material (such as TMOs and TMOHs) with HER catalyst to facilitate water dissociation, introducing hydrogen adsorption material into ZAB catalyst may facilitate the kinetic of water splitting of OER and deprotonation process of ORR in neutral condition. [98] [99] For example, Subbaraman *et al*. has proposed a bifunctional metal-metal oxide system to facilitate the water splitting in alkaline environment. By depositing $Ni(OH)_2$ clusters on Pt surface in which metal-oxide $Ni(OH)_2$ was responsible for facilitating the dissociation of water and the metal for adsorption of produced atomic hydron, the activity for HER was increased by a factor of eight.[100]

Although this review focuses on the interface engineering of heterostructured air electrocatalysts for Zn-air battery, the fundamental understanding of the interface chemistry in terms of geometric structure, coordination structure, and electronic structure also shed light on the rational design of heterostructured electrocatalysts for board electrochemical applications. Thus, we hope that this review will bring significant attention in the field of electrochemistry, by enabling more frontier researches in the fields of battery technology.

Acknowledgements

This work is supported by National Natural Science Foundation of China (Grant No. 51722105), National Key Research and Development Program (SQ2019YFE010807) and Zhejiang Provincial Natural Science Foundation of China (LR18B030001).

Received: ((will be filled in by the editorial staff))
Revised: ((will be filled in by the editorial staff))
Published online: ((will be filled in by the editorial staff))

References

[1] M. Armand, J. M. Tarascon, *Nature* **2008**, *451*, 652.

[2] J. Fu, R. Liang, G. Liu, A. Yu, Z. Bai, L. Yang, Z. Chen, *Adv. Mater.* **2019**, *31*, 1805230.

[3] A. S. Aricò, P. Bruce, B. Scrosati, J.-M. Tarascon, W. Schalkwijk, *Nat. Mater.* **2005**, *4*, 366.

[4] C. Yang, J. Chen, X. Ji, T. P. Pollard, X. Lü, C.-J. Sun, S. Hou, Q. Liu, C. Liu, T. Qing, Y. Wang, O. Borodin, Y. Ren, K. Xu, C. Wang, *Nature* **2019**, *569*, 245.

[5] Y. Jiang, Y. Li, W. Sun, W. Huang, J. Liu, B. Xu, C. Jin, T. Ma, C. Wu, M. Yan, *Energy Environ. Sci.* **2015**, *8*, 1471.

[6] Y. Jiang, Y. Li, P. Zhou, Z. Lan, Y. Lu, C. Wu, M. Yan, *Adv. Mater.* **2017**, *29*, 1606499.

[7] J. B. Goodenough, Y. Kim, *Chem. Mater.* **2010**, *22*, 587.

[8] J. M. Tarascon, M. Armand, *Nature* **2001**, *414*, 359.

[9] L. Fang, C. Wang, L. Huangfu, N. Bahlawane, H. Tian, Y. Lu, H. Pan, M. Yan, Y. Jiang, *Adv. Funct. Mater.* **2019**, *29*, 1906680.

[10] A. Manthiram, Y. Fu, Y.-S. Su, *Acc. Chem. Res.* **2013**, *46*, 1125.

[11] G. Fang, J. Zhou, A. Pan, S. Liang, *ACS Energy Lett.* **2018**, *3*, 2480.

[12] Y. Li, H. Dai, *Chem. Soc. Rev.* **2014**, *43*, 5257.

[13] T. Liu, J. P. Vivek, E. W. Zhao, J. Lei, N. Garcia-Araez, C. P. Grey, *Chem. Rev.* **2020**, *120*, 6558.

[14] J. Fu, Z. P. Cano, M. G. Park, A. Yu, M. Fowler, Z. Chen, *Adv. Mater.* **2017**, *29*, 1604685.

[15] X. Chen, Z. Zhou, H. E. Karahan, Q. Shao, L. Wei, Y. Chen, *Small* **2018**, *14*, 1801929.

[16] D. U. Lee, P. Xu, Z. P. Cano, A. G. Kashkooli, M. G. Park, Z. Chen, *J. Mater. Chem. A* **2016**, *4*, 7107.

[17] C. Han, W. Li, H.-K. Liu, S. Dou, J. Wang, *Mater. Horiz.* **2019**, *6*, 1812.

[18] E. Davari, D. G. Ivey, *Sustainable Energy Fuels* **2018**, *2*, 39.

[19] G. Fu, Y. Tang, J.-M. Lee, *ChemElectroChem* **2018**, *5*, 1424.

[20] Y. Zhong, X. Xu, W. Wang, Z. Shao, *Batteries Supercaps* **2019**, *2*, 272.

[21] J. Zhang, Q. Zhou, Y. Tang, L. Zhang, Y. Li, *Chem. Sci.* **2019**, *10*, 8924.

[22] G. Zhao, K. Rui, S. X. Dou, W. Sun, *J. Mater. Chem. A* **2020**, *8*, 6393.

[23] X. Long, W. Qiu, Z. Wang, Y. Wang, S. Yang, *Mater. Today Chem.* **2019**, *11*, 16.

[24] L. An, Z. Zhang, J. Feng, F. Lv, Y. Li, R. Wang, M. Lu, R. B. Gupta, P. Xi, S. Zhang, *J. Am. Chem. Soc.* **2018**, *140*, 17624.

[25] Z. Huang, X. Qin, X. Gu, G. Li, Y. Mu, N. Wang, K. Ithisuphalap, H. Wang, Z. Guo, Z. Shi, G. Wu, M. Shao, *ACS Appl. Mater. Interfaces* **2018**, *10*, 23900.

[26] B. Chen, Z. Jiang, J. Huang, B. Deng, L. Zhou, Z.-J. Jiang, M. Liu, *J. Mater. Chem. A* **2018**, *6*, 9517.

[27] H.-F. Wang, C. Tang, Q. Zhang, *Adv. Funct. Mater.* **2018**, *28*, 1803329.

[28] Z. W. Seh, J. Kibsgaard, C. F. Dickens, I. Chorkendorff, J. K. Nørskov, T. F. Jaramillo, *Science* **2017**, *355*, eaad4998.

[29] Y. Chen, S. Ji, C. Chen, Q. Peng, D. Wang, Y. Li, *Joule* **2018**, *2*, 1242.

[30] Y. Yang, M. Luo, W. Zhang, Y. Sun, X. Chen, S. Guo, *Chem* **2018**, *4*, 2054.

[31] F. Wang, P. He, Y. Li, T. A. Shifa, Y. Deng, K. Liu, Q. Wang, F. Wang, Y. Wen, Z. Wang, X. Zhan, L. Sun, J. He, *Adv. Funct. Mater.* **2017**, *27*, 1605802.

[32] K. He, T. Tadesse Tsega, X. Liu, J. Zai, X.-H. Li, X. Liu, W. Li, N. Ali, X. Qian, *Angew. Chem., Int. Ed.* **2019**, *58*, 11903.

[33] K. Wang, Z. Mo, S. Tang, M. Li, H. Yang, B. Long, Y. Wang, S. Song, Y. Tong, *J. Mater. Chem. A* **2019**, *7*, 14129.

[34] M. Luo, S. Guo, *Nat. Rev. Mater.* **2017**, *2*, 17059.

[35] M. Buongiorno Nardelli, B. I. Yakobson, J. Bernholc, *Phys. Rev. B* **1998**, *57*, R4277.

[36] X.-R. Wang, J.-Y. Liu, Z.-W. Liu, W.-C. Wang, J. Luo, X.-P. Han, X.-W. Du, S.-Z. Qiao, J. Yang, *Adv. Mater.* **2018**, *30*, 1800005.

[37] M. Busch, N. B. Halck, U. I. Kramm, S. Siahrostami, P. Krtil, J. Rossmeisl, *Nano Energy* **2016**, *29*, 126.

[38] G. Zhao, P. Li, N. Cheng, S. X. Dou, W. Sun, *Adv. Mater.* **2020**, *32*, 2000872.

[39] C. Zhao, Y. Li, W. Zhang, Y. Zheng, X. Lou, B. Yu, J. Chen, Y. Chen, M. Liu, J. Wang, *Energy Environ. Sci.* **2020**, *13*, 53.

[40] C. B. Roxlo, B. Abeles, T. Tiedje, *Phys. Rev. Lett.* **1984**, *52*, 1994.

[41] J. Grunes, J. Zhu, G. A. Somorjai, *Chem. Commun.* **2003**, 2257.

[42] C. Zhu, S. Fu, Q. Shi, D. Du, Y. Lin, *Angew. Chem., Int. Ed.* **2017**, *56*, 13944.

[43] Y. Peng, B. Lu, S. Chen, *Adv. Mater.* **2018**, *30*, 1801995.

[44] Z. Jiang, W. Sun, H. Shang, W. Chen, T. Sun, H. Li, J. Dong, J. Zhou, Z. Li, Y. Wang, R. Cao, R. Sarangi, Z. Yang, D. Wang, J. Zhang, Y. Li, *Energy Environ. Sci.* **2019**, *12*, 3508.

[45] J. Shen, Y. Zhu, Y. Hu, C. Li, *Mater. Today Nano* **2018**, *4*, 54.

[46] J. Su, R. Ge, Y. Dong, F. Hao, L. Chen, *J. Mater. Chem. A* **2018**, *6*, 14025.

[47] B.-Q. Li, C.-X. Zhao, S. Chen, J.-N. Liu, X. Chen, L. Song, Q. Zhang, *Adv. Mater.* **2019**, *31*, 1900592.

[48] T. Kwon, M. Jun, J. Joo, K. Lee, *J. Mater. Chem. A* **2019**, *7*, 5090.

[49] L. Carbone, P. D. Cozzoli, *Nano Today* **2010**, *5*, 449.

[50] Y. Ma, J. Li, X. Liao, W. Luo, W. Huang, J. Meng, Q. Chen, S. Xi, R. Yu, Y. Zhao, L. Zhou, L. Mai, *Adv. Funct. Mater.* **2020**, 2005000.

[51] T. Zhou, N. Zhang, C. Wu, Y. Xie, *Energy Environ. Sci.* **2020**, *13*, 1132.

[52] B. Kim, A. Oh, M. K. Kabiraz, Y. Hong, J. Joo, H. Baik, S.-I. Choi, K. Lee, *ACS Appl. Mater. Interfaces* **2018**, *10*, 10115.

[53] X. Liu, K. Ni, C. Niu, R. Guo, W. Xi, Z. Wang, J. Meng, J. Li, Y. Zhu, P. Wu, Q. Li, J. Luo, X. Wu, L. Mai, *ACS Catal.* **2019**, *9*, 2275.

[54] G. Zhao, K. Rui, S. X. Dou, W. Sun, *Adv. Funct. Mater.* **2018**, *28*, 1803291.

[55] X. Liu, M. C. Hersam, *Adv. Mater.* **2018**, *30*, 1801586.

[56] P. Das, Q. Fu, X. Bao, Z.-S. Wu, *J. Mater. Chem. A* **2018**, *6*, 21747.

[57] J. Su, G.-D. Li, X.-H. Li, J.-S. Chen, *Adv. Sci.* **2019**, *6*, 1801702.

[58] Z.-F. Huang, J. Song, X. Wang, L. Pan, K. Li, X. Zhang, L. Wang, J.-J. Zou, *Nano Energy* **2017**, *40*, 308.

[59] J. Lv, S. C. Abbas, Y. Huang, Q. Liu, M. Wu, Y. Wang, L. Dai, *Nano Energy* **2018**, *43*, 130.

[60] R. Zhang, W. Jian, Z.-D. Yang, F.-Q. Bai, *Chin. Chem. Lett.* **2020**, *31*, 2319.

[61] J. Low, J. Yu, M. Jaroniec, S. Wageh, A. A. Al-Ghamdi, *Adv. Mater.* **2017**, *29*, 1601694.

[62] C. Zhou, S. Wang, Z. Zhao, Z. Shi, S. Yan, Z. Zou, *Adv. Funct. Mater.* **2018**, *28*, 1801214.

[63] S. Zhou, M. Wen, N. Wang, Q. Wu, Q. Wu, L. Cheng, *J. Mater. Chem.* **2012**, *22*, 16858.

[64] J. Deng, D. Deng, X. Bao, *Adv. Mater.* **2017**, *29*, 1606967.

[65] J. Deng, P. Ren, D. Deng, X. Bao, *Angew. Chem., Int. Ed.* **2015**, *54*, 2100.

[66] D. Deng, L. Yu, X. Chen, G. Wang, L. Jin, X. Pan, J. Deng, G. Sun, X. Bao, *Angew. Chem., Int. Ed.* **2013**, *52*, 371.

[67] S. Guo, X. Pan, H. Gao, Z. Yang, J. Zhao, X. Bao, *Chem. - Eur. J.* **2010**, *16*, 5379.

[68] M. Zeng, Y. Liu, F. Zhao, K. Nie, N. Han, X. Wang, W. Huang, X. Song, J. Zhong, Y. Li, *Adv. Funct. Mater.* **2016**, *26*, 4397.

[69] C. Korte, A. Peters, J. Janek, D. Hesse, N. Zakharov, *Phys. Chem. Chem. Phys.* **2008**, *10*, 4623.

[70] V. J. Parks, A. J. Durelli, *Exp. Mech.* **1967**, *7*, 279.

[71] L. A. Kibler, A. M. El-Aziz, R. Hoyer, D. M. Kolb, *Angew. Chem., Int. Ed.* **2005**, *44*, 2080.

[72] S. Schnur, A. Groß, *Phys. Rev. B* **2010**, *81*, 033402.

[73] J. Zhang, M. B. Vukmirovic, Y. Xu, M. Mavrikakis, R. R. Adzic, *Angew. Chem., Int. Ed.* **2005**, *44*, 2132.

[74] L. Bu, N. Zhang, S. Guo, X. Zhang, J. Li, J. Yao, T. Wu, G. Lu, J.-Y. Ma, D. Su, X. Huang, *Science* **2016**, *354*, 1410.

[75] W. Xiao, M. A. Liutheviciene Cordeiro, M. Gong, L. Han, J. Wang, C. Bian, J. Zhu, H. L. Xin, D. Wang, *J. Mater. Chem. A* **2017**, *5*, 9867.

[76] D. Yan, Y. Li, J. Huo, R. Chen, L. Dai, S. Wang, *Adv. Mater.* **2017**, *29*, 1606459.

[77] L. An, Y. Li, M. Luo, J. Yin, Y.-Q. Zhao, C. Xu, F. Cheng, Y. Yang, P. Xi, S. Guo, *Adv. Funct. Mater.* **2017**, *27*, 1703779.

[78] J. Bao, X. Zhang, B. Fan, J. Zhang, M. Zhou, W. Yang, X. Hu, H. Wang, B. Pan, Y. Xie, *Angew. Chem., Int. Ed.* **2015**, *54*, 7399.

[79] T. Ling, D.-Y. Yan, Y. Jiao, H. Wang, Y. Zheng, X. Zheng, J. Mao, X.-W. Du, Z. Hu, M. Jaroniec, S.-Z. Qiao, *Nat. Commun.* **2016**, *7*, 12876.

[80] J. Yin, Y. Li, F. Lv, Q. Fan, Y.-Q. Zhao, Q. Zhang, W. Wang, F. Cheng, P. Xi, S. Guo, *ACS Nano* **2017**, *11*, 2275.

[81] Y. Jiang, Y.-P. Deng, J. Fu, D. U. Lee, R. Liang, Z. P. Cano, Y. Liu, Z. Bai, S. Hwang, L. Yang, D. Su, W. Chu, Z. Chen, *Adv. Energy Mater.* **2018**, *8*, 1702900.

[82] B. Y. Guan, Y. Lu, Y. Wang, M. Wu, X. W. Lou, *Adv. Funct. Mater.* **2018**, *28*, 1706738.

[83] M. Zhang, Q. Dai, H. Zheng, M. Chen, L. Dai, *Adv. Mater.* **2018**, *30*, 1705431.

[84] B. Lu, Q. Liu, S. Chen, *ACS Catal.* **2020**, *10*, 7584.

[85] Y. Li, B. Jia, Y. Fan, K. Zhu, G. Li, C.-Y. Su, *Adv. Energy Mater.* **2018**, *8*, 1702048.

[86] M. Wu, M. Cui, L. Wu, S. Hwang, C. Yang, Q. Xia, G. Zhong, H. Qiao, W. Gan, X. Wang, D. Kline, M. R. Zachariah, D. Su, T. Li, L. Hu, *Adv. Energy Mater.* **2020**, *10*, 2001119.

[87] J. Chen, H. Li, C. Fan, Q. Meng, Y. Tang, X. Qiu, G. Fu, T. Ma, *Adv. Mater.* **2020**, *32*, 2003134.

[88] J. Wang, J. Liu, B. Zhang, H. Wan, Z. Li, X. Ji, K. Xu, C. Chen, D. Zha, L. Miao, J. Jiang, *Nano Energy* **2017**, *42*, 98.

[89] W. Niu, S. Pakhira, K. Marcus, Z. Li, J. L. Mendoza-Cortes, Y. Yang, *Adv. Energy Mater.* **2018**, *8*, 1800480.

[90] Y. Chen, S. Ji, S. Zhao, W. Chen, J. Dong, W.-C. Cheong, R. Shen, X. Wen, L. Zheng, A. I. Rykov, S. Cai, H. Tang, Z. Zhuang, C. Chen, Q. Peng, D. Wang, Y. Li, *Nat. Commun.* **2018**, *9*, 5422.

[91] D. Ji, L. Fan, L. Li, S. Peng, D. Yu, J. Song, S. Ramakrishna, S. Guo, *Adv. Mater.* **2019**, *31*, 1808267.

[92] Z. K. Yang, C.-Z. Yuan, A.-W. Xu, *ACS Energy Lett.* **2018**, *3*, 2383.

[93] J. Zhang, M. Zhang, Y. Zeng, J. Chen, L. Qiu, H. Zhou, C. Sun, Y. Yu, C. Zhu, Z. Zhu, *Small* **2019**, *15*, 1900307.

[94] J. Zhao, R. Qin, R. Liu, *Appl. Catal., B* **2019**, *256*, 117778.

[95] P. Peng, L. Shi, F. Huo, C. Mi, X. Wu, S. Zhang, Z. Xiang, *Sci. Adv.* **2019**, *5*, eaaw2322.

[96] C. Tang, B. Wang, H.-F. Wang, Q. Zhang, *Adv. Mater.* **2017**, *29*, 1703185.

[97] L. Zhang, Y. Jia, G. Gao, X. Yan, N. Chen, J. Chen, M. T. Soo, B. Wood, D. Yang, A. Du, X. Yao, *Chem* **2018**, *4*, 285.

[98] B. Zhang, J. Liu, J. Wang, Y. Ruan, X. Ji, K. Xu, C. Chen, H. Wan, L. Miao, J. Jiang, *Nano Energy* **2017**, *37*, 74.

[99] X. Zhang, Y. Liang, Adv. Sci. **2018**, *5*, 1700644.

[100] R. Subbaraman, D. Tripkovic, D. Strmcnik, K.-C. Chang, M. Uchimura, A. P. Paulikas,

V. Stamenkovic, N. M. Markovic, *Science* **2011**, *334*, 1256.

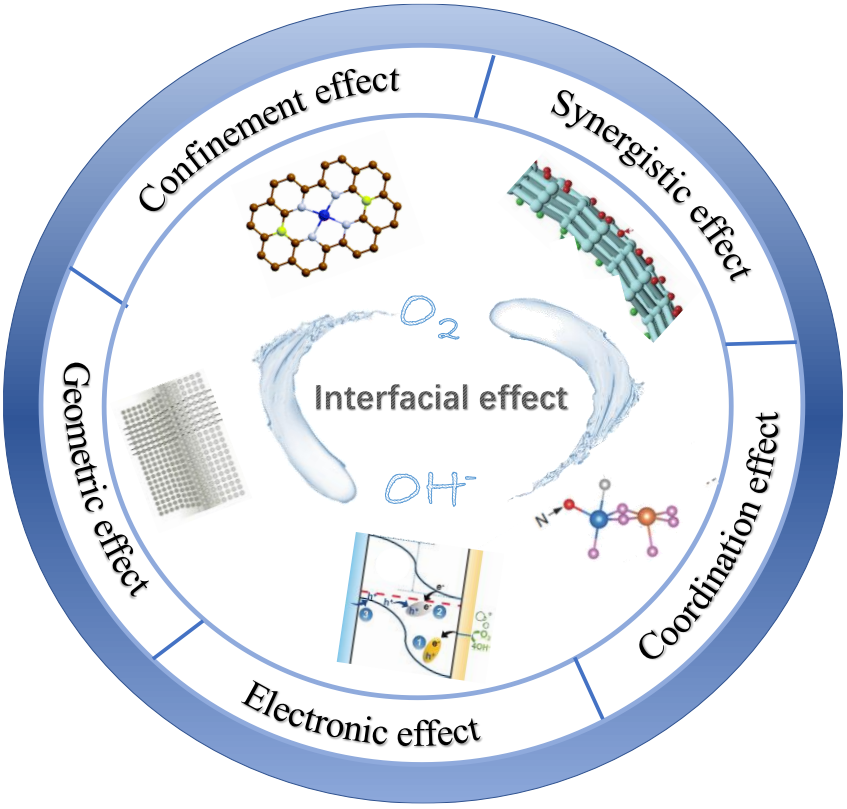

Figure 1. Schematic illustration of interfacial effects.

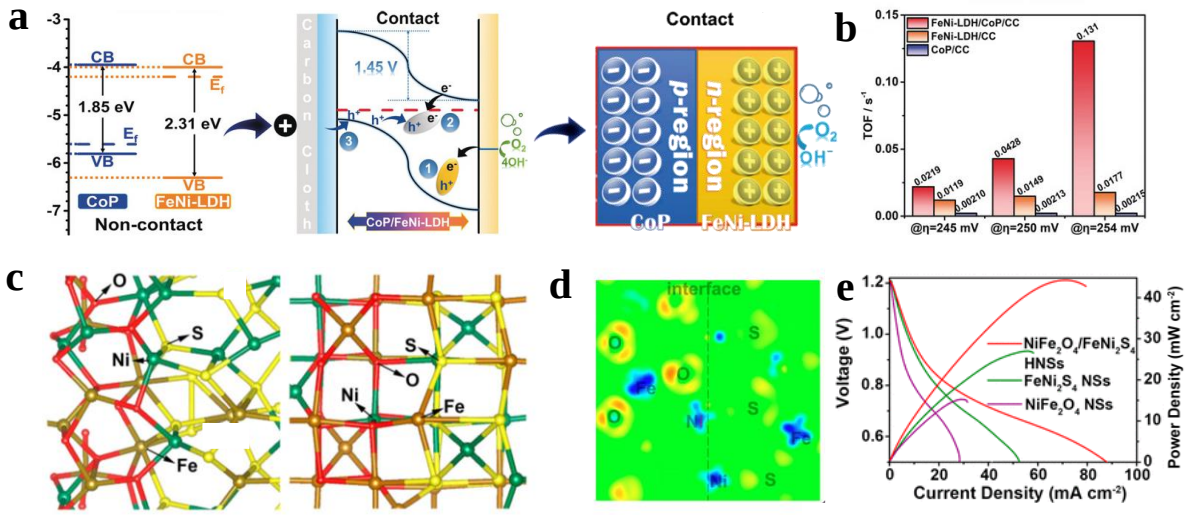

Figure 2. (a) The energy diagrams of CoP and FeNi-LDH and the proposed mechanism for OER in the FeNi-LDH/CoP p-n junction. (b) Turnover frequency (TOF) at different overpotentials. Reproduced with permission. [32] Copyright 2019, Angew. Chem. Int. Ed. (c) Constructed two $NiFe_2O_4/FeNi_2S_4$ interface models, $NiFe_2O_4/FeNi_2S_4$-(311) model (left) and $NiFe_2O_4/FeNi_2S_4$-(100) model (right). (d) Differential charge density of the cross-sectional view of the $NiFe_2O_4/FeNi_2S_4$-(311) interface model. The red/light (blue/dark) areas mark an increase (decrease) of the electron density. (e) Polarization and power density curves of neutral RZABs with $NiFe_2O_4/FeNi_2S_4$, $FeNi_2S_4$, and $NiFe_2O_4$ as air-cathodes. Reproduced with permission. [24] Copyright 2018, J. Am. Chem. Soc.

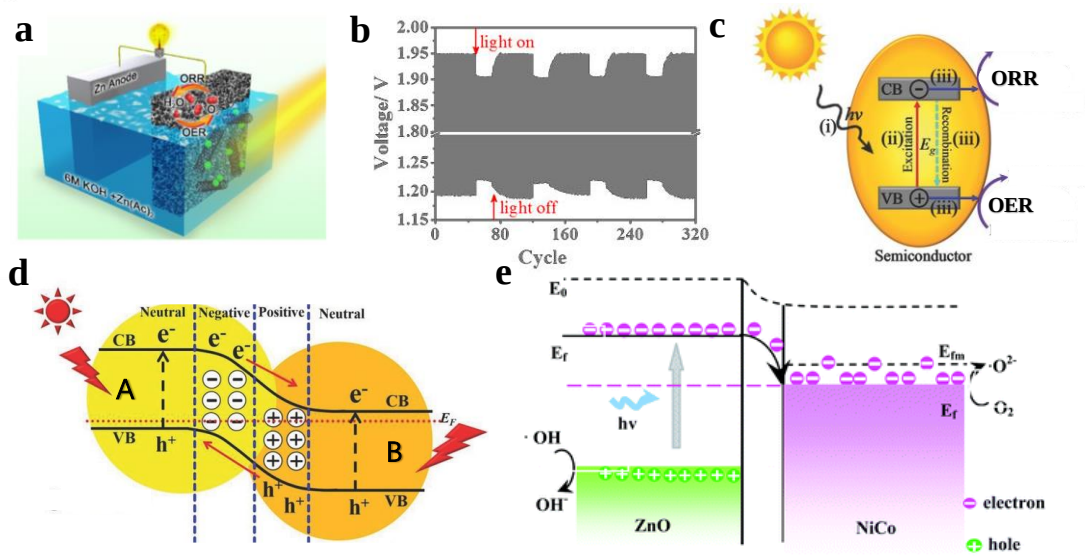

Figure 3. (a) Schematic representation of the rechargeable photo-enhanced Zn-air battery. (b) Galvanostatic discharge-charge cycling curves at 10 mA cm^{-2} of the rechargeable Zn-air battery equipped with the $Ni_{12}P_5$@NCNT catalyst in the dark and under ~ 1 sun illumination, respectively. Reproduced with permission. [59] Copyright 2018, Nano Energy. (c) Schematic illustration of the photocatalytic processes on a semiconductor. (d) Schematic illustration of the electron-hole separation of a p-n heterojunction photocatalyst under light irradiation. Reproduced with permission. [61] Copyright 2017, Adv. Mater. (e) The photocatalytic mechanism of the metal-semiconductor system under visible-light illumination. Reproduced with permission. [63] Copyright 2012, J. Mater. Chem.

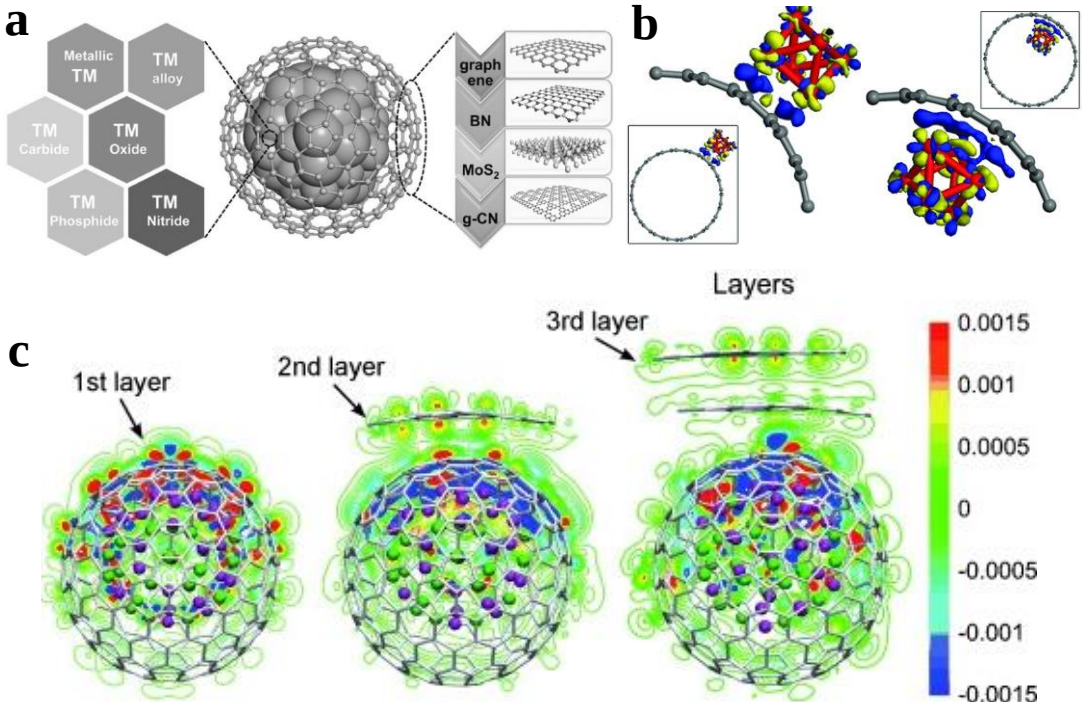

Figure 4. (a) Schematic illustration of chainmail catalyst. Reproduced with permission. [64] Copyright 2017, Adv. Mater. (b) Isosurface of the differential electron density for Ru_6-out-CNT and Ru_6-in-CNT. Reproduced with permission. [67] Copyright 2010, Chem. Eur. J. (c) Redistribution of the electron densities when metal clusters have covered by one to three layers of graphene. Reproduced with permission. [65] Copyright 2015, Angew. Chem. Int. Ed.

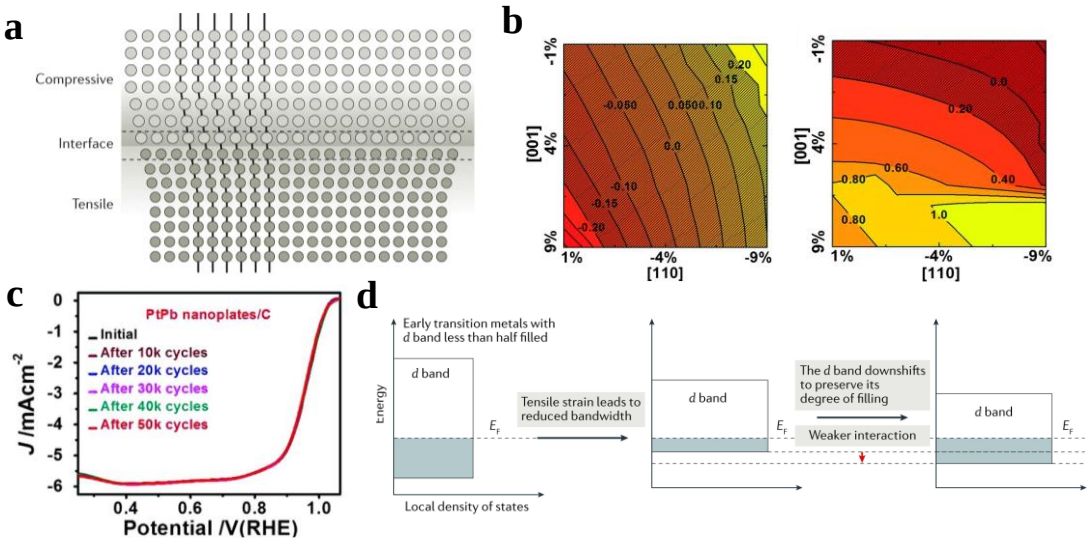

Figure 5. (a) A schematic of the strain field influenced by lattice mismatch at the interface between two metals with different lattice parameters. Reproduced with permission. [69] Copyright 2008, Phys. Chem. Chem. Phys. (b) Relative oxygen binding energy (ΔE_O) as a function of biaxial strain in the [110] and [001] directions for the proposed active sites on Pt (110) facets. The optimal ΔE_O value is set to 0. (c) ORR polarization curves of the PtPb nanoplates/C catalyst before and after different potential cycles. Reproduced with permission. [74] Copyright 2016, Science. (d) Energy diagrams explaining the influence of tensile strain on the position of the d band in early transition metals. Reproduced with permission. [72] Copyright 2010, Phys. Rev. B.

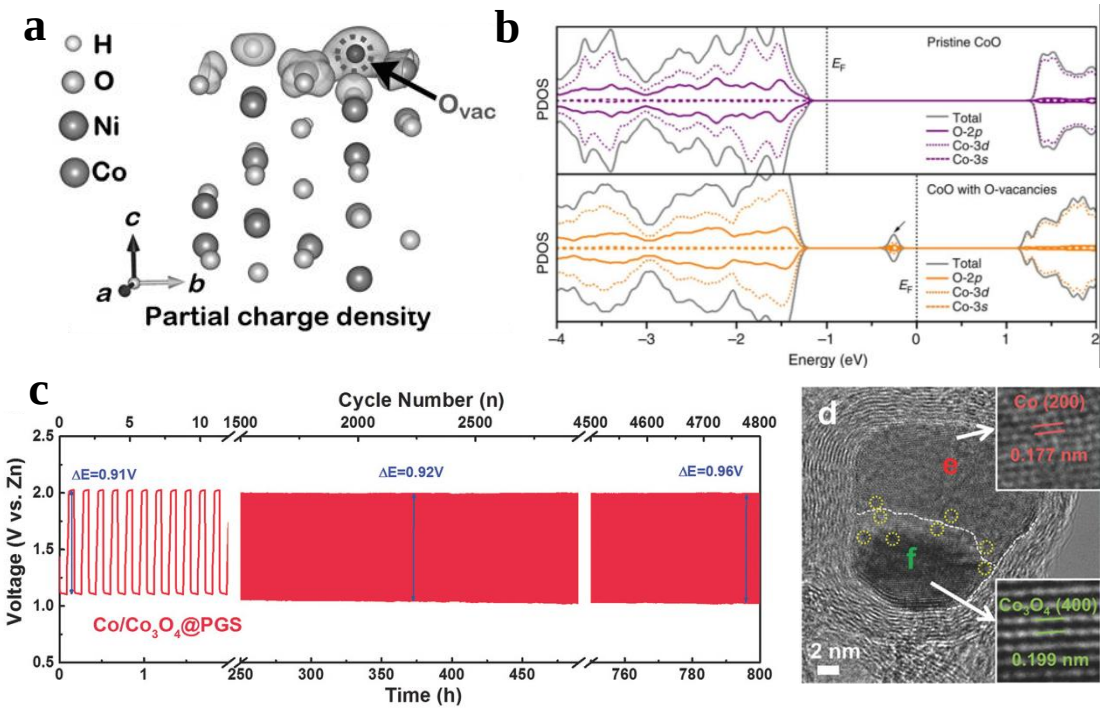

Figure 6. (a) The partial charge density of $NiCo_2O_4$ with oxygen vacancies. Reproduced with permission. [78] Copyright 2015, Angew. Chem. (b) The projected density of states (PDOS) on pristine CoO and CoO with O-vacancies. The arrow in b points new electronic states. Reproduced with permission. [79] Copyright 2016, Nat. Commun. (c) Galvanostatic cycling stability of Zn-air battery with Co/Co_3O_4@PGS catalysts at a current density of 10 mA cm^{-2}. (d) HRTEM images of a single nanoparticle Co/Co_3O_4@PGS, in which (e) represents Co region and (f) represents Co_3O_4 region. Reproduced with permission. [81] Copyright 2018, Adv. Energy Mater.

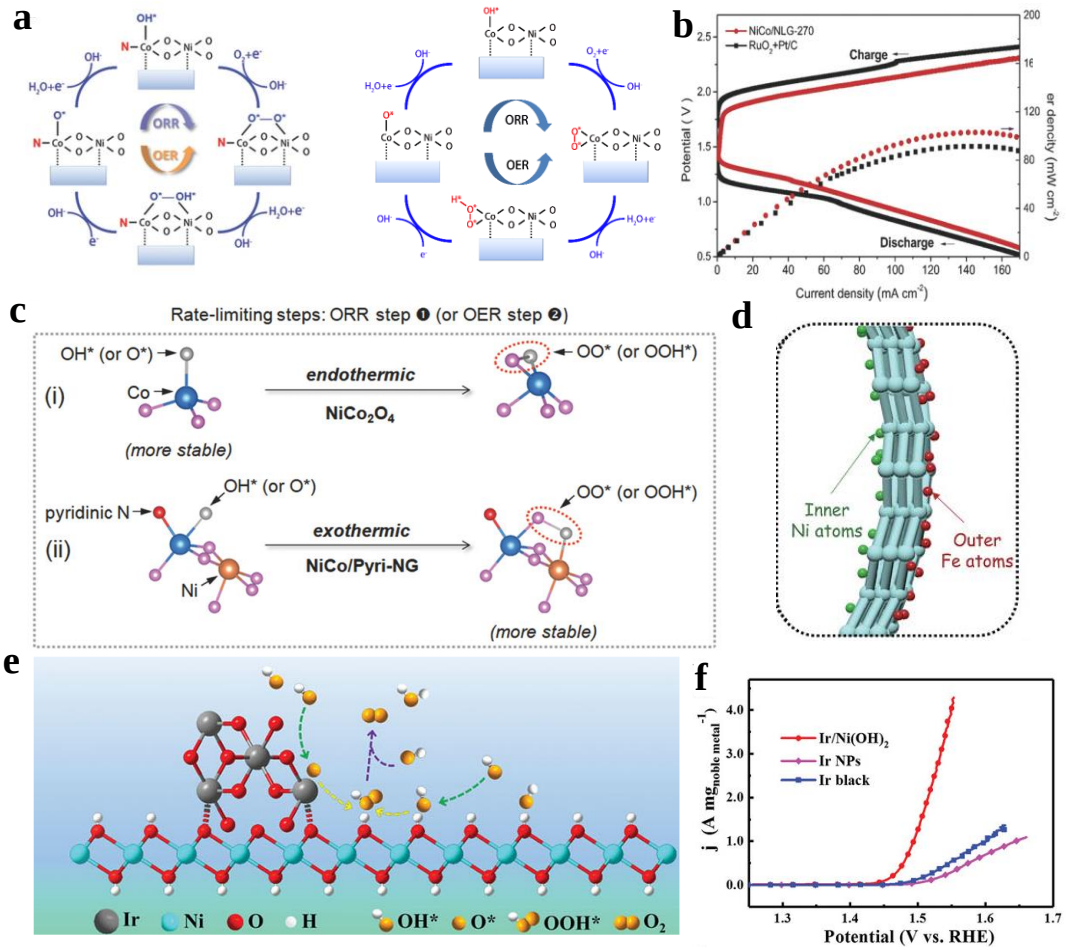

Figure 7. (a) ORR (clockwise) and OER (anticlockwise) mechanisms of catalyst before and after coordinating with pyridinic N. (b) Galvanodynamic charge/discharge profiles and power density curves of NiCo/NLG-270 and Pt/C + RuO_2 catalyst. (c) Adsorption configurations of oxygen containing species on the Co site of $NiCo_2O_4$ before and after coordinating with pyridinic N. Reproduced with permission. [36] Copyright 2018, Adv. Mater. (d) Scheme of the Ni-N_4/GHSs/Fe-N_4 catalyst. Reproduced with permission. [87] Copyright 2020, Adv. Mater. (e) Illustration of the proposed OER mechanism based on synergistic effect. (f) Ir mass-normalized LSV curves of Ir/$Ni(OH)_2$. Reproduced with permission. [38] Copyright 2020, Adv. Mater.

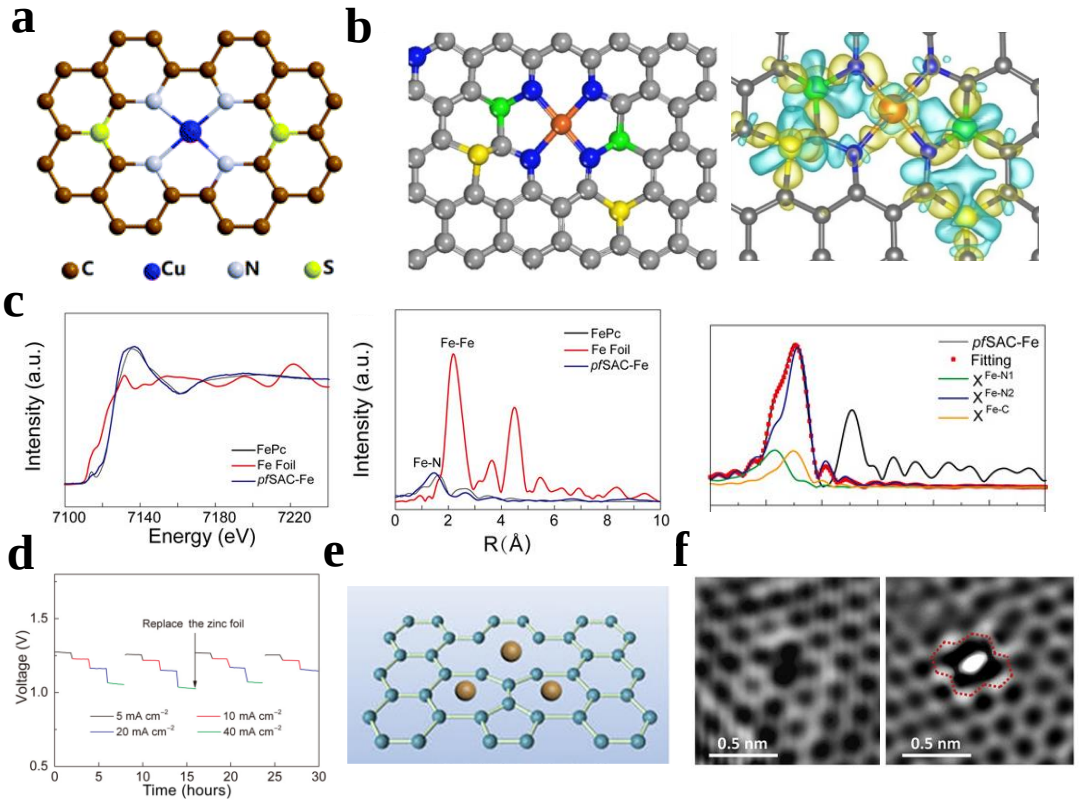

Figure 8. (a) Schematic interfacial model of SAC. The atomic interface related to SACs refers to the interface between the isolated metal-atoms and the support. Reproduced with permission. [44] Copyright 2019, Energy Environ. Sci. (b) Schematic model of single iron atomic sites dispersed in N, P, S co-doped carbon polyhedron and the corresponding calculated charge density differences, Fe (orange), N (blue), P (green), S (yellow) and C (gray). Reproduced with permission. [90] Copyright 2018, Nat. Commun. (c) X-ray absorption fine structure (XAFS) spectroscopy of pfSAC-Fe. (d) Cycle discharge curves of Zn-air batteries at periodically changed current densities of 5, 10, 20, and 40 mA cm^{-2}. Reproduced with permission. [86] Copyright 2019, Sci. Adv. (e) Schematic illustration of metal atom trapped by defect. (f) The zoomed-in image of the defective area (with atomic Ni trapped). The Di-vacancy is marked with the red dashed line. Reproduced with permission. [97] Copyright 2017, Chem.

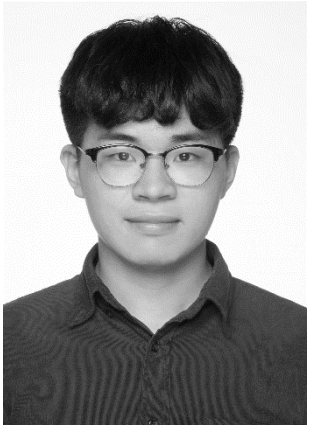

Minghe Luo received his Bachelor degree in Material Science and Engineering from Ningbo University in 2018. He is currently a master student under the supervision of Prof. Jiang at Zhejiang University. His research interests focus mainly on energy materials and electrochemistry for zinc-based batteries.

Wenping Sun is professor at School of Materials Science and Engineering, Zhejiang University. He received his B.S. in 2008 and Ph.D. in materials science in 2013 from the University of Science and Technology of China (USTC). His research expertise includes electrocatalysis, fuel cells, and batteries, especially the design of novel materials and structures, and fundamental understanding of related electrochemical processes.

Ben B. Xu is a Professor of Materials and Mechanics in the Department of Mechanical and Construction Engineering at Northumbria University, UK. Ben obtained his Ph.D in Mechanical Engineering(2011) at Heriot-Watt University in Edinburgh, then moved to the University of Massachusetts, Amherst (US), to work(2011-2013) with Prof. Ryan C. Hayward as a postdoc. Ben's research interests include materials chemistry, responsive materials, soft matter physics, mechanics and micro-engineering. He has published 1 US patent, 1 book chapter and 70+ journal articles, including *Nat. Commun.*, *Adv. Mater.*, *Adv. Fun. Mater.*, *Energy. Environ. Sci.*, *Nano Energy*, *Phys. Rev. Lett.*, *Small*., etc.

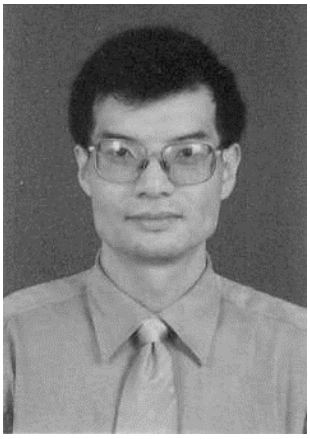

Hongge Pan received his PhD in Materials Science and Engineering from Zhejiang University in 1996 under a joint program between Zhejiang University and Institute of Physics, Chinese Academy of Science. Later that year he joined Zhejiang University and became a Professor in 1999. His research is focused on energy materials for solid-state hydrogen storage and lithium batteries.

Yinzhu Jiang is a full professor at School of Materials Science and Engineering in Zhejiang University, China. He received his Ph.D. degree in Department of Materials Science and Engineering from University of Science and Technology of China in 2007. He worked as a post-doctoral researcher in Heriot-Watt University, United Kingdom from 2007 to 2008 and an Alexander von Humboldt Fellow in Bielefeld University, Germany from 2008 to 2010. His research interests focus mainly on energy-related materials and electrochemistry, including rechargeable batteries, metal anodes and solid electrolytes.

This review focus on how interface engineering improves the intrinsic activity of catalysts and how to enable the stabilization of metal species when particle size is downsized to single atoms. The well-established interface-kinetic relationship in this review highlight the unique attribute of interface and provide important insights into the mechanism of performance enhancement, establishing scientific basis towards new heterostructured electrocatalysts design.

M.H. Luo, W.P. Sun, B. Xu, H.G. Pan, Y.Z. Jiang*

Interface Engineering of Air Electrocatalysts for Rechargeable Zinc-Air Batteries